Article:
Das, C orcid.org/0000-0002-1454-6210, Elguweri, M, Jiang, P et al. (8 more authors) (2019) Controlled Synthesis, Characterization, and Flow Properties of Ethylene–Diene Copolymers. Macromolecular Reaction Engineering, 13 (3). 1800071. ISSN 1862-832X

https://doi.org/10.1002/mren.201800071

DOI: 10.1002/mren.((insert number))
Article Type ((Full Paper)

Controlled synthesis, characterization, and flow-properties of ethylene-diene copolymers

Chinmay Das*, Muhiddin Elguweri, Peijun Jiang, Shuhui Kang, Mauritz Kelchtermans, Tom C. B. McLeish, Matthew Parkinson, Daniel J. Read*, Michael P. Redlich, Pradeep P. Shirodkar, Johannes M. Soulages

---

Dr. Chinmay Das, Prof. Daniel J. Read
School of Mathematics
University of Leeds,
Leeds LS2 9JT, United Kingdom
E-mail: c.das@leeds.ac.uk, d.j.read@leeds.ac.uk

Muhiddin Elguweri, Dr. Mauritz Kelchtermans, Dr. Matthew Parkinson
Advanced Characterization
ExxonMobil Chemical Europe,
Hermeslaan 2, B-1831 Machelen, Belgium

Dr. Peijun Jiang, Dr. Shuhui Kang, Dr. Pradeep P. Shirodkar
Global Chemical Research
ExxonMobil Chemical
Baytown, TX 77520, USA

Prof. Tom C. B. McLeish
Department of Physics,
University of York,
York, YO10 5DD, United Kingdom

Michael P. Redlich, Dr. Johannes M. Soulages
Corporate Strategic Research,
ExxonMobil Research and Engineering Company,
Annandale, NJ 08801, USA

The flow response of branched entangled resins is dominated by the branching topology of the constituent molecules, a property that is not directly accessible using experimental analytical tools for industrially relevant complex resins. In this paper, we report the controlled terpolymerization of ethylene, 1,9-decadiene, and either hexene or octene in a continuous stirred tank reactor with a metallocene catalyst. The synthesized samples were characterized

extensively with various analytical tools and their rheological properties were measured with small amplitude oscillatory shear and start-up uniaxial extension experiments. A model was developed for the polymerization process with the mass balance during synthesis providing strong constraints on the rate constants. *In silico* ensembles of molecules, generated via Monte Carlo sampling, were used to reproduce the experimental results. The computer model allows us to infer the detailed branching structure of the molecules and to predict the optimum range of reactor conditions for this synthesis.

FIGURE FOR ToC_ABSTRACT

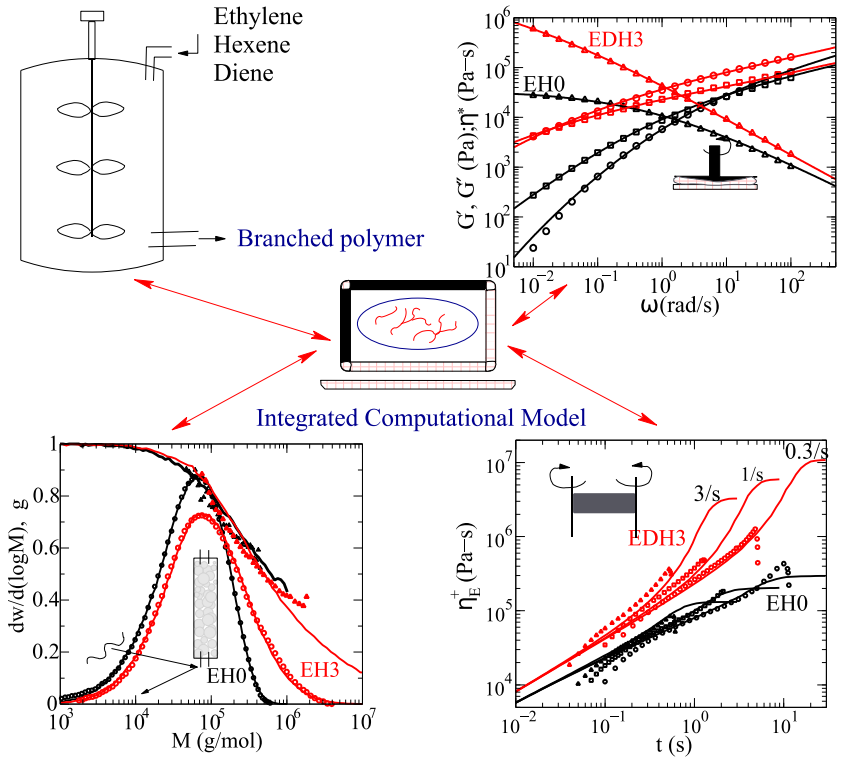

1. Introduction

Polymers containing long-chain-branching (LCB) offer efficient processing[1-3] and account for the dominant use of low-density polyethylene (LDPE) synthesized at high pressure in current industrial practice. However, the free radical polymerization scheme for LDPE synthesis generates a broad distribution of molar mass, short and long-chain branches with little independent control on the molar mass and the concentration of short and long-chain branches. In contrast, recent advances in constrained geometry catalysts,[4] for example metallocene catalysts,[5] allow for homogeneous placement of different comonomers and precise control of the molar mass. Many metallocene catalysts also generate branched molecules by incorporating vinyl-ended chains (macromonomer).[6, 7] The very small concentration of such macromonomers compared to the concentration of monomers leads to sparse LCB. Also, the presence of hydrogen in the reactor can lead to the saturation of the vinyl chain-ends and frustrate the possibility of LCB. An alternate strategy to increase the amount of LCB is the copolymerization using non-conjugated dienes[8, 9] that create pendant double bonds at the incorporation sites along the growing chain and provide a controllable number of multiple branching sites as opposed to a unique branching site at the termination-end of a macromonomer.

The pendant dienes create “H-shaped” links connecting two linear segments, which can lead to gelation[10, 11] with increasing diene concentration. Since the polymerization of the linear segments at the catalyst sites and the insertion of a pendant diene into another growing chain happen in the same reactor, the probability of forming a LCB depends on the time spent by a particular molecule in the reactor. Molecules residing for a long time in the reactor will eventually have all the pendant dienes incorporated into other chains (i.e. reacted on both ends). In contrast, molecules that exit the reactor immediately after being synthesized will have all the

pendant dienes unreacted. This dependence of reaction-probability on the residence time of a particular molecule leads to different molar mass distributions in continuous stirred tank reactors (CSTR) and in semi-batch reactors.[12] The gelation transition in semi-batch reactor follows classical mean-field behavior. In particular, the weight-averaged molar mass diverges as a power-law function of the reduced distance to the gel-point. A number of existing synthesis[13-17] and modeling[18-20] studies focus on this semi-batch reaction of α-olefin (ethylene or propylene) with non-conjugated dienes.

The approach to gelation in a CSTR for this reaction is qualitatively different. Early theoretical studies[21] considered a method of moment approach with a closure hypothesis connecting the second moment of the molar mass to higher moments. At a certain diene concentration, the solution of the approximated equations fails to predict a real root for the weight averaged molar mass and is identified as the gel-point. Many of the subsequent theoretical studies[16, 18, 19] retained the closure approximation, while introducing more complexity in the description of the reaction steps. In a recent publication,[12] we used Monte Carlo simulations to show that the exponential distribution of residence times of the molecules synthesized in a CSTR and the residence time dependence of the probability for branch formation at the pendant dienes lead to molar mass distributions with power-law tails with the power-law exponent demanding finite values of the first three moments of the molar mass at gelation. Since the commonly measured number, weight, and z-averaged molar masses are predicted to be finite at the gel-point, a direct experimental determination of gelation is quite difficult, if not impossible.

Compared to the synthesis in semi-batch conditions, very little has been published so far on the synthesis of ethylene-diene polymers in a CSTR. Only the published work by Guzman et al.[16] considers the CSTR synthesis of ethylene/ decadiene/ octene terpolymers. They analyzed the

molar mass distributions of the synthesized polymers using theoretical predictions[21] based on the method of moments and noted the difficulty in predicting the onset of gelation for this reaction.

In this work, we present results from the well-controlled synthesis of terpolymers in a CSTR using ethylene, 1,9-decadiene, and either hexene or octene. We extensively characterized the resins using calorimetry, size-exclusion chromatography with light scattering and viscometry, crystallization elution fractionation, nuclear magnetic resonance, as well as linear and non-linear rheology. A minimal Monte Carlo (MC) model that captures the complexity of the synthesis is used to integrate the results from the various experiments. The MC model allows us to get insight about the underlying branching architecture, to predict the rheological properties, and to predict the maximum diene concentration beyond which controlled synthesis of this polymer is not possible.

2. Experiments

2.1 **Polymerization**

Materials: Polymerization grade ethylene, 1-hexene, 1-octene, 1,9-decadiene and solvent (isohexane) were supplied by pipeline from the ExxonMobil chemical plant and purified by passing through an Oxiclear column (model RGP-R1-500 from Labelear) followed by a 5Å and a 3Å molecular sieve columns. Dimethylsilyl-bis-(tetrahydroindenyl)zirconium dichloride was used as the metallocene catalyst, N,N-dimethyl anilinium tetrakis(heptafluoro-2-naphthyl)borate as the activator, and tri-n-octyl aluminum (25 wt% in hexane, Sigma Aldrich) diluted in isohexane as the impurity scavenger. The catalyst was pre-activated at a molar ratio of 1:1 in toluene and kept in an inert atmosphere with less than 1.1ppm water content.

Synthesis: A 1L stainless steel autoclave reactor equipped with a stirrer, a water cooling/steam heating element with a temperature controller, and a pressure controller was used for the syntheses. The reactor was purged with nitrogen at the maximum allowed temperature and then by pumping isohexane and scavenger solution through the reactor for at least one hour. The temperature and the pressure respectively were fixed to 130℃ and 2 MPa. Monomers and catalyst solutions were then fed into the reactor after cooling down to -15℃ by passing through a chiller. The solvent flow rate was set to 54g/min for all cases (resulting in a residence time of $\tau_{res} \approx 12$ minutes). The ethylene supply was regulated to 8 slpm (standard liter per minute) and the catalyst was added at a rate of 3.27×10^{-8} mol/min. The comonomer and 1,9-decadiene flow rates for synthesizing the different samples are shown in **Table 1**. The sample EH0 was synthesized with hexene as comonomer and without using any diene. The series EDH1-3 contains hexene as comonomer at a fixed feed rate with increasing amount of diene across the samples. The series EDO1-3 was synthesized with identical diene feed, but with increasing rate of octene feed. Scavenger solution flow rate was adjusted to achieve a maximum catalyst activity. Once the activity reached steady state, the operation was continued for at least five times the mean residence time before the samples were collected, air-dried in a hood and then in a vacuum oven at 90℃ for 12 hours. Online IR detectors were used to monitor both the monomer and comonomer conversions.

2.2 **Blending with metallocene linear low density polyethylene**

The diene terpolymer EDH1 was solution blended in xylene with a commercial linear (low density) polyethylene (EHL) at weight fractions 9%, 23%, and 33% using a twin screw DSM microcompouder and a Haake mixer (ThermoFisher). EHL is a gas-phase metallocene

polymer with M_W=117.7 Kg/mol, PDI=2.6, and contains 1.9 mole% of hexene as comonomer.

2.3 **Characterization**

Differential scanning calorimetry (DSC): DSC measurements were done using a TA Instruments model Q200 DSC applying 10 ℃/min heating and cooling rates. All samples were analyzed under a N_2 purge. Lower and upper temperature limits were -50 and 220 ℃ respectively. The numbers reported in **Table 2** are from the second melt.

Size Exclusion Chromatography (SEC): SEC experiments were done using three mixed Polymer Laboratories Mixed B columns at a nominal 0.5 ml/min flow rate with a nominal 0.45 mg injected mass. The mobile phase and operating temperature were 1,2,4 trichlorobenzene and 145 ℃, respectively. The SEC equipment was an Agilent 220C high temperature instrument equipped with an online differential refractomer (DRI), a multi-angle light scattering (MALLS), and a viscometer detector. The DRI and viscometer (four capillary design) were inherent to the Agilent SEC. The MALLS detector was an eighteen angle Wyatt Technology HELEOS II with a nominal 657 nm laser. The details for the detector design and calibration are described elsewhere.[22, 23]

A protocol combining the DRI calibration curve for the low molar mass end (high elution volume), the molar mass as determined by LS detector where the concentration is high enough to ensure reliable mass measurements, and a polynomial fit of the molar mass as determined from LS to the elution volume at the highest molar mass end was used to determine the reported molar mass distributions and the molar mass moments.

Crystallization Elution Fractionation (CEF): Chemical composition distributions were measured using a Polymer ChAR Crystallization Elution Fractionation (CEF) instrument[24] equipped with an IR4 infrared detector to measure concentration. The solvent was 1,2 dichlorobenzene. The crystallization was done with a 0.5 ℃/min cooling rate with a 0.008 ml/min flow rate, cooling down to -10 ℃. The elution step was done with a 1.0 ℃/min heating rate with a 0.5 ml/min flow rate. The CEF was calibrated with narrow composition distribution ethylene-hexene copolymers to convert temperature to mole% comonomer.

Nuclear Magnetic Resonance (NMR): All ^{1}H and $^{13}C\{^{1}H\}$ NMR spectra[25, 26] were recorded using a Bruker Advance-III 600 NMR spectrometer operating at 600.23 and 150.93 MHz for ^{1}H and ^{13}C respectively. All spectra were recorded using a ^{13}C optimized 10 mm DUL extended temperature cryo-probehead at 125 °C using nitrogen gas for all pneumatics. Approximately 200 mg of material was dissolved in 2 mL of 1,2,4-trichlorobenzene (TCB) using additional benzene-d6 for field locking. The sample was measured without sample rotation.

For $^{13}C\{^{1}H\}$ spectra standard single-pulse excitation was employed with NOE, a 11.5 s recycle delay and a bilevel WALTZ65 decoupling scheme. A total of 5120 (5k) transients were acquired per spectra. This setup was chosen primarily for the high resolution and sensitivity needed for detection of microstructure elements in low concentration. As well as the expected *B4 site observed at 38.16 ppm the *B6+ site from long-branches was observed at 38.22 ppm.

The long-chain branch content was quantified in units of branches per thousand total carbons based on the integral ratio of the *B6+ and δ sites compensating for the presence of B4 branching originating from hexene, as quantified by the integral of the *B4 site. Slope and bias correction was needed for the *B6+ integral. Due to the combination of low signal intensity of the *B6+ site and its overlap with *B4 and its associated ^{13}C satellite, precision of

quantification is admittedly limited. It should be noted that measurements for the absolute contents of LCB in PE is not trivial due to a lack of standardization. Thus the values of LCB content are reported in this paper for relative comparison with comparability ensured by use of the same sample concentration and acquisition parameters. By the same argument the order of magnitude reported here are valid. The calculation of absolute error[27-29] in the measured LCB content requires separation of the random aspects of the signal from the noise to provide an estimation of the error of the quantitative integral (error in bulk integral can be taken to be negligible). However, often in such cases more error is introduced by assumption than confidence gained by manipulation,[27-29] and the raw values and example spectra, as presented in this paper, are more informative. That said the quantities obtained serve to illustrate general trends and order of magnitude.

2.4 **Rheology**

Small amplitude oscillatory shear (SAOS) experiments: The linear viscoelastic responses of the samples were obtained with an Advanced Rheometric Expansion System (ARES) rheometer using 25 mm parallel plate geometry. Samples were stabilized and compression-molded to ~1mm thickness discs under vacuum at 190℃. For all samples, frequency sweeps were performed at 190℃ in the frequency range $0.01 < \omega < 100$ rad/s. For selected samples, the shear rheology measurements were performed at temperatures between 150℃ and 210℃. The different temperature data does not superpose perfectly showing lack of exact time-temperature-superposition (TTS). All measurements were performed under nitrogen atmosphere to minimize degradation and care was taken to be in the linear regime.

Transient uniaxial extensional response: To measure the extensional rheology response, selected samples were compression molded into thin rectangular strips with dimensions 18mm × 5mm and thickness ≈ 1mm. Uniaxial extensional rheology was performed at 150℃

under nitrogen atmosphere on the selected samples by using the SER fixture (Sentmanat Elongational Rheometer, Xpansion Instruments) mounted on the shear rheometer. Inherent limitations for the SER fixture allow to reach a maximum Hencky strain of 4.

3. Modelling

The different experimental characterization techniques used in this work provide bulk information for the samples, averaged over all the molecules. We use computer modelling to integrate these experimental observations to resolve detailed branching structures of the individual molecules. Detailed branching structures also enable us to predict the flow properties of the samples. Once the parameters of the computer model are optimized by comparing with the experimental results, such models can be used to guide synthesis intended for specific desired flow properties. Our modelling approach involves the generation of *in silico* molecules from consideration of the reactor conditions and reaction steps; interrogating the computer generated molecules to calculate various ensemble averages (for example branch-point density) or distributions (for example molar mass distribution); and to predict the linear and non-linear rheology.

3.1 **Reaction Steps**

We consider simple reaction kinetics based on earlier work on polymerization of polyethylene with a single-site metallocene catalyst[7] supplemented by additional steps involving the reaction of a bifunctional diene.[30] The details of the scheme, except additional steps

considered to model the non-ideality of the experimental reactor, have been reported elsewhere.[12] In addition to the diene, the experimental work also includes copolymerization with another α-olefin comonomer (such as hexene or octene). When the distinction between the monomer and the comonomer is made, the monomer we refer to is always ethylene, and the comonomer is the second α-olefin. However, the catalyst used in this work incorporates comonomer randomly and uniformly (see results from CEF in section 4.3), and the reactions are performed under steady state conditions, justifying the consideration of comonomers in a preaveraged sense, i.e. we can consider the effective "averaged" polymerization rate for an "averaged" effective monomer, where the averaging is performed over monomer and comonomer. Hence, the rate constants in our description are effective (pseudo-kinetic) rate constants[31] that may depend on the comonomer type and concentration. The concentration of incorporated diene always remains much lower than that of ethylene or comonomer (less than 0.18 dienes per 1000 ethylene). Thus, we neglect the effect of the diene concentration on the rate constants and on altering the effective mass of the averaged effective "monomer". The alternative approach, in which separate rate constants are used for reaction of comonomer and monomer, requires the introduction of many more parameters, but can be reduced to an effective average rate constant under steady state conditions[31].

The reaction scheme in reference[12] considers that a growing chain incorporates a "monomer" with a rate constant k_{p} or a diene with a rate constant k_{pD}. The chain terminates with a terminal double bond with rate $k^{=}$ and these vinyl-ended chains act as macromonomers that are incorporated into a growing chain with rate constant k_{PLCB} giving rise to three-functional long-chain branches. We also consider that a fraction of the growing chains terminate without a terminal double bond with rate k_{s}. Incorporated dienes introduce pendant double bonds which may be incorporated into growing chains with a rate constant k_{DLCB} generating four-functional long-chain branches.

We first consider the data and theory in the absence of diene. Resins generated in an idealized CSTR with a single site metallocene catalyst have been predicted to be described by just two independent parameters (typically one characterizing the molar mass and another characterizing the branching).[32] However, comparing our experimental data with this idealized theoretical approach (see Appendix A), we found two major discrepancies. Firstly, comparing the theoretical molar mass distribution to the experimental one for the diene-free sample, we found that the synthesis resulted in a greater than expected proportion of low molar mass molecules (Appendix A, Figure 11a). Secondly, the width of the sample molar mass distribution provides an indication of the number of LCB (noting that polymerization of purely linear molecules under ideal CSTR conditions may be expected to result in a Flory distribution of chain lengths with dispersity of 2, whilst introduction of LCB through macromonomer incorporation increases the predicted dispersity above 2).[32] However, the NMR experiments provide an independent measure of the number of long-chain branches. The number of long-chain branches required to describe the observed width of the molar mass distribution (Appendix A, Figure 11a), using the theory for idealized polymerization in a CSTR,[32] is approximately *half* of the value suggested from NMR experiments.

The above two deviations from the idealized CSTR prediction may be resolved by hypothesizing a single deviation from ideality: that the polymerization conditions additionally produce a small subpopulation of short, linear macromonomers (explaining the higher than expected low molar mass molecules in the experimental synthesis), some of which are incorporated into other growing chains (explaining the high LCB content observed in NMR without increasing the width of the MWD). The presence of such shorter molecules can be rationalized by considering local high concentration of monomers close to the monomer inlet and the resulting higher probability of transfer to monomer leading to larger termination rate. Our fitted termination rate constants support such bi-molecular termination events (Appendix

B, Figure 13c). We next discuss the details of this hypothesis and its effect on our polymerization model.

We may first examine the deviation from the idealized MWD by adding in an excess component of low molar mass molecules to the theoretical prediction. We find that the required distribution has a small weight fraction of ~6% and a polydispersity very close to 2, suggesting that the excess molecules are mostly linear. An appropriately weighted superposition of a single site metallocene branched resin and a metallocene linear resin (having PDI=2.0) can describe the molar mass distribution but does not improve on the predictions for the LCB density (the NMR results) or the strain hardening in uniaxial extension (see Appendix A). Good agreements with the NMR measurements and the non-linear flow responses are only possible if we assume that some of the short linear molecules act as macromonomers, so that the population of short chains couples to the synthesis of long chains. For computational simplicity, we model this situation by considering a subpopulation of catalyst having a different set of rate constants. To keep the changes in the algorithm developed for the ideal CSTR minimal, we assume that this 2nd catalyst does not incorporate long-chain branches or diene, i.e. it forms only linear chains. This is justified since local high monomer concentration would mean relative rarity of diene and macromonomers.

3.2 **Monte Carlo Sampling**

Our assumption that the second catalyst only produces linear molecules that can be incorporated by the primary catalyst requires only minor changes in the algorithm described in reference [12]. For simplicity, we characterize the second catalyst by different termination rate constants while keeping the addition rate constant (k_{p}) and the monomer concentration the same as that of the primary catalyst. Like the primary catalyst, we consider two different termination rates, $k_2^{=}$ and k_{s2}, corresponding to rates for terminating with a vinyl chain end

and a saturated chain end, respectively. The relative molar fraction of the second catalyst, φ_{Y2} is used as a fitting parameter. With our approximations, the probability of selecting a random reacted monomer in the produced resin that had been polymerized by the second catalyst will be the same as the mole fraction of the second catalyst φ_{Y2}. When the selected monomer is from the 2nd catalyst, there are no branches in the upstream direction (towards the chain end where polymerization starts). In the downstream direction (towards the termination end), reincorporation by a live chain growing at a later time (by the primary catalyst) is considered. The relative concentration of macromonomer generated from the 2nd catalyst is given by $k_2^{=}\varphi_{Y2}/[\, k_2^{=}\varphi_{Y2} + \, k^{=}(1-\varphi_{Y2})]$ and this sets the probability of an incorporated macromonomer being synthesized by the 2nd catalyst.

We average over 5×10^5 molecules for calculating the static properties such as MWD and density of LCB. To calculate the flow properties, we bin the generated molecules in logarithm of the molar mass and aim for similar number of molecules in each bin by removing excess molecules and assigning their weights to the surviving molecules in bins having a large number of molecules. Typically, rheology calculations employed $\sim$25000 molecules. The *in silico* ensemble for the linear polymer EHL was created by directly discretizing the GPC-determined molar mass distribution.

3.3 **Computational Rheology**

We calculate the linear viscoelastic and the startup uniaxial responses of the molecules generated by the algorithm outlined above by using the publicly available computational rheology software BoB-rheology.[33-35, 3]

Details of the algorithm have been published elsewhere.[33, 34] Briefly, within the tube model,[36] each strand of a given molecule is imagined to be confined in a tube like region due to the topological constraint created by all other molecules. The macroscopic deformation is

assumed to induce an affine deformation at the length-scale of the tube diameter. The resulting stress can only decay once the molecules have the chance to escape from the deformed tube and sample new, equilibrium orientations. The dominant relaxation pathway for linear polymer is reptation[37] – i.e. a one dimensional diffusion along the tube axis. For a star-branched molecule, the presence of a branch-point prohibits diffusion. Instead, the relaxation proceeds following a much slower, activated arm-retraction mechanism. For a generic branch-on-branch polymer, once the outermost arms have relaxed, their effect is included in the relaxation of the next level of inner branches by assigning localized friction points along the chain.[38] Typically, during the last step of relaxation for a branch-on-branch polymer, the confined innermost strand behaves like a linear molecule with additional localized friction points from the outer, already relaxed segments; and can reptate away in the final relaxation step.

In the melt, the tube constraint arises from the molecules themselves. The fast relaxing molecules (or fast relaxing segments) act like a solvent, which softens the tube potential (dilates the tube). This dynamic dilution[39] couples the relaxation of the different molecules in polydisperse (either in molar mass, or in architecture, or in both) polymer melts: the relaxation of a certain molecule is coupled to the relaxation of all other molecules. For randomly branched industrial resins, computational rheology[40, 33, 34, 41] provides an efficient way to track the relaxation of molecules with topological complexity.

To calculate the linear viscoelastic response, we start with a numerical representation of the "molecules" retaining the strand molar mass and the branching topology information. The ensemble of molecules needs to be large enough to capture the complexity of the resin of interest. The algorithm follows the relaxation in discrete time steps after an imposed small step strain deformation. At each time step, the tube theory predictions are numerically solved to determine which parts of the molecules have already relaxed, consistent with the current

tube diameter. The new tube diameter is calculated from the surviving weight fraction of unrelaxed molecules. The time dependence of the fraction of molecules carrying stress and the tube diameter is used to compute the viscoelastic moduli.

The algorithm for calculating the linear rheology also assigns orientational and stretch relaxation times (taken to be an effective Rouse time) to individual segments forming a particular molecule. The ensemble of molecules is mapped to a set of pompom modes[42] with these known relaxation times and priorities (maximum tension that the backbone of an equivalent pompom molecule can sustain in an extensional flow) calculated based on the molecular topology.[34] Because of the tube dilation, the priorities depend on the flow rate.[3, 34] The pompom constitutive model is numerically solved to calculate the transient rheological response in uniaxial extensional flow.

The rheology model involves two chemistry dependent parameters: the entanglement molar mass M_e, and the entanglement time τ_e. The entanglement molar mass M_e is related to the plateau modulus G_0 via $G_0 = \frac{4}{5}\frac{\rho RT}{M_e}$. Here, ρ is the mass density of the polymer, R is the universal gas constant and T is the absolute temperature. We used $\rho = 0.76$ g/cc at 190℃ and 0.784 g/cc at 150℃. Experiments suggest that M_e for copolymers of ethylene and α-olefins vary systematically with the effective monomer molar mass M_0.[43] For the comonomer content in our samples, the suggested relation is $M_e = 1120 \times \left(\frac{M_0}{28}\right)^{3.49}$ g/mol. Here we have used the value of M_e for ethylene homopolymers as 1120 g/mol.[33] The entanglement time τ_e varies sensitively with comonomer content.[44] We use τ_e as a fitting parameter for each sample to fit the low frequency viscous response measured using small amplitude oscillatory shear experiments. The dependence of τ_e on the comonomer content is discussed at the end of section 4.5.

There are several parameters/choices in the rheology model that are believed to be chemistry independent. We used all other such parameters as in our previous studies on different branched polymers.[33, 34, 3, 30] In particular, we set the 'hopping parameter' associated with the branch point friction to $p^2 = \frac{1}{40}$. When a significant fraction of chains relax quickly, the tube diameter increases comparatively slowly via constraint release Rouse relaxation and can be described using a "supertube".[33, 40] During such times, the arm retraction is considered in the 'supertube'.

4. Results

4.1 **Molar mass distribution and thermal properties**

Table 2 shows the molar mass moments determined from SEC-MALLS, viscosity averaged viscosity contraction factor g′, crystallization and melting temperatures, and enthalpy of crystallization for the different samples. The full molar mass distributions are shown in figure 3 and 4. The thermodynamic properties are consistent with previous studies[45] on ethylene-hexene and ethylene-octene copolymers with similar comonomer contents. Monotonically decreasing values of g′ with increasing diene content in the ethylene-hexene-diene samples indicate increasing LCB. However, the small variation in g′ across the samples only reflects a marginal increase in the average number of LCB.

4.2 **Unsaturation and branching from NMR**

Figure 1 shows the ^{13}C NMR spectrum for EDH1. The number of LCB is estimated using the ratio of the area under the peak at 38.22 ppm (from LCB) to that at 38.16 ppm (from hexene comonomer). The small separation of the two peaks introduces significant uncertainty in the computed LCB content from the choice of the integration windows and the base line. The

numbers of LCB/1000C and the numbers of terminal and internal double bonds for the samples with hexene as comonomer are given in **Table 3**.

4.3 **Comonomer distribution**

Figure 2(a) shows the concentration of material crystallized as a function of temperature for EH0 obtained from CEF. The relative concentration of molecules as a function of the mole fraction of hexene is shown in Figure 2(b). The distribution is sharply peaked indicating a homogeneous incorporation of the comonomer during the polymerization process. This allows us to incorporate the comonomer in an averaged sense in our MC model.

4.4 **Rate constants and molecular structures**

The ethylene (C_2) and the comonomer (C_X) feed rates, their conversions and the residence time suffice to determine the ethylene and comonomer concentrations in the reactor. The concentration of the active catalyst [Y] is proportional to the catalyst flow rate. If we assume that [Y] is a constant, the addition rate constants for C_2 and C_X vary appreciably (~40% for C_2 and ~30% for C_X) between the samples without any systematic dependence on the concentration or the type of the comonomer. However, the addition rate constants C_2 and C_X calculated by assuming a fixed value of [Y] for the different samples show a linear correlation between themselves (Figure 13a in Appendix B). This suggests that the main variation between the samples is the varying amount of active catalyst during the synthesis of the different samples. Some degree of uncertainty in [Y] is expected between the different syntheses because of the extreme sensitivity of the catalyst to any impurity in the feed and the necessity of precisely maintaining a very low flow rate for the catalyst. We arbitrarily fix [Y]=10^{-6} mol/L for the synthesis of EH0 (a different choice of [Y] will result in different values of the rate constants without affecting their ratios which determine the molecular architectures). This choice of [Y] gives $k_{\mathrm{p,C2}} = 3.02 \times 10^4$ L/mol-s and $k_{\mathrm{p,C6}} = 2.43 \times 10^3$

L/mol-s from the molar conversions of ethylene and hexene. Treating the comonomer in an average sense, we define the effective monomer concentration [M] as the sum of ethylene (molar) concentration [C_2] and the comonomer concentration [C_X]. The effective propagation rate constant k_p is determined by demanding that the molar conversion is the sum of the ethylene and comonomer conversions. The individual propagation rate constants and the concentrations also give the mole fraction of comonomer incorporated in the samples and thus the effective monomer molar mass M_0.

For the sample EH0, we used the mole fraction of the 2nd catalyst (the fraction of catalyst responsible for synthesizing short linear polymers near the monomer inlet), the termination rates and the macromonomer incorporation rate constant as fitting parameters to simultaneously fit the molar mass distribution from SEC, the number of terminal double bonds per 1000 carbon, and the number of long-chain branches per 1000 carbon determined from NMR. The number of LCB is affected by both the proportion of chains terminated with a vinyl-end ($k^{=}/[k^{=} + k_s]$) and the macromonomer incorporation rate constant k_{PLCB}. We can get very good fit for the molar mass distribution and the number of LCB with very different k_{PLCB} by varying the proportion of chains terminated with a vinyl-end. However, to simultaneously match the NMR determined number of terminal double bonds and the number of LCB, a choice of $k_{PLCB} \approx 3.5\, k_{p,CX}$ is required. Such larger addition rate constants for macromonomers compared to smaller α-olefins have been found in earlier studies[46, 47] and have been ascribed to local higher concentration of macromonomers near the catalysts. The best fit for EH0 required the termination rates for the primary catalyst $k^{=} = 4.32$/s, $k_s = 4.15$/s, the mole fraction of the 2nd catalyst $\varphi_{Y2} = 0.16$, and the termination rates for the 2nd catalyst $k_2^{=} = 29.17$/s, and $k_{s,2} = 8.18$/s. This choice of rate constants gives the number of vinyl ends per thousand carbons as 0.13 and number of LCB/1000C as 0.39.

To describe all of the other resins, we fix the ratio of the total termination rates between the two catalysts (ratio of $k_T \equiv k^{=} + k_s$, and $k_{T,2} \equiv k_2^{=} + k_{s,2}$) to be the same as for EH0. We also keep the ratio of the vinyl-termination rate to the total termination rate for individual catalysts ($\frac{k^{=}}{k_T} = 0.51$ for the primary catalyst and $\frac{k_2^{=}}{k_{T,2}} = 0.78$ for the 2nd catalyst) constant and identical to that of EH0. The value of k_T is varied to best fit the molar mass distribution for each sample. Because of the relatively large uncertainty in determining the number of LCB in NMR, we have not used the NMR results in fitting the samples except for EH0. The fitted values of k_T for the different samples show a linear dependence on the monomer concentration (Figure 13c in Appendix B) suggesting a contribution in the termination rate from the transfer to monomer. Since both the hexene and the octene copolymerization can be described by the same propagation rate constant, and direct detection of diene consumption is difficult due to the small concentration of diene involved in the synthesis, we assume that $k_{PD} = k_{p,CX}$. With this choice of the diene propagation rate constant, fitting the molar mass distribution of EDH1 gives $k_{DLCB} = 0.7 \times 10^3$ L/mol-s.

The mole fraction of the 2nd catalyst, the (total) termination rate for the primary catalyst k_T, and the catalyst concentration [Y] were varied for the remaining samples to fit the molar mass distributions. Though we treat k_T as a separate fitting parameter, the presence of a linear relationship between k_T and the monomer concentration shows that each individual sample actually requires only two independent fitting parameters – the mole fraction of the 2nd catalyst (related to higher concentration at the inlet), and the active catalyst concentration (possibly due to variability in catalyst poisoning and small variation in the catalyst flow rate between the different syntheses). The fitted values of the mole fraction of the 2nd catalyst, the termination rate constant and the catalyst concentration for the different samples are shown in **Table 4**. We also show the number of LCB/1000C (λ), number of LCB/molecule (b_m), number of terminal double bonds ($n^{=}$) and the effective monomer molar mass (M_0) in Table

4. The predicted LCB in Table 4 for the diene containing samples are lower than those predicted from NMR. The signature from the pendant dienes cannot be resolved from those of rheologically active LCB in NMR measurements. Incorporating the pendant dienes in the LCB count in the modelling gives good agreement with the NMR results except for EDH3. A table containing this comparison is presented in Appendix C.

The average number of diene induced 4-functional branches is much smaller than the macromonomer induced 3-functional branches even for the highest diene feed rates considered. For EDH3, the number of 3-functional branches per 1000C is 0.29 and the number of 4-functional branches per 1000C is 0.02. However, the pendant dienes contribute significantly in increasing the number of terminal double bonds. For EDH3, the total number of terminal double bonds per 1000C is 0.17, of which 0.07 is due to the pendant once-reacted dienes. On average only 0.09 of the diene molecules are incorporated per 1000 backbone carbon. Our fits assign increasing values of the number of branches per molecule with increasing diene flow rate. However, the variation in the monomer concentration and the termination rate generates different molar mass segments in the different samples. Thus, the number of LCB/1000C is not a monotonically increasing function of the diene flow-rate.

Figure 3 and 4 show the experimental data (from SEC-MALLS) and the model predictions for the molar mass distributions and the radius of gyration contraction factors (g-factor) for the samples containing hexene and octene, respectively.

4.5 **Flow response in small amplitude oscillatory shear and uniaxial extension**

Figure 5 and **figure 6** show the experimental results and model predictions for the linear viscoelastic response of the samples at 190℃ containing hexene and octene as comonomer, respectively. The entanglement molar mass M_e for these samples were determined from the

effective "monomer" molar mass M_0. For each of the samples, the entanglement time τ_e was independently chosen to match the low-frequency viscosity.

Figure 7 shows the transient extensional stress growth coefficients for the resins containing hexene as comonomer. For these experiments, the samples break before reaching a Henky strain of 2.5. The model predictions are in agreement with the experimental data.

Figure 8 shows the dynamic viscosity for blends of EDH1 in EHL at different weight fractions. Beyond the reptation time for EHL, the relaxation of the branched EDH1 molecules proceed in a dilated tube. The comparison between the experiments and model predictions show that the model does not quantitatively capture the detailed frequency behavior close to the reptation time of the linear matrix (around frequency 10 rad/s).

In our modelling, we have treated τ_e as a fitting parameter for the linear rheology data. **Figure 9** shows the values of τ_e used for all the different samples and the blends as a function of the entanglement molar mass M_e. We have also included the data for comonomer free metallocene polyethylene in the plot.[33] Experimentally, the zero shear viscosities for a series of linear ethylene/α-olefin copolymers at fixed weight-averaged molar mass were found to be independent of the comonomer content.[48] This observation coupled with the backbone molar mass dependence of the plateau modulus[43] suggests that τ_e should vary as a power-law with exponent 4.6 with M_e.[44] Our results suggest a much stronger dependence of τ_e on M_e and hence on the backbone molar mass. Loops formed by incorporation of both ends of a diene molecule by the same polymer may play a role in increasing τ_e.[30]

4.6 **Maximum diene concentration for reproducible synthesis**

Two different considerations are important for the controlled synthesis of diene copolymers. Firstly, with increasing diene concentration, the molar mass diverges leading to gel formation with possibility of reactor fouling. In **figure 10**(a) we show the calculated Z+1 moment (4th

moment) of the molar mass as a function of the diene feed flow rate. For these calculations, we have assumed that the monomer and the comonomer flow rates are the same as those of the synthesis of EH0, $\varphi_{Y2} = 0.16$, and [Y]=10^{-6} mol/L. The termination rate constant is calculated as $k_T = 2.26 + 21.14\,[M]$ (see figure 13c in Appendix B). A power-law fit of the data ($M_{Z+1} \sim (1 - I_D / I_D^*)^{-\gamma}$) gives the critical diene flow-rate $I_D^* = 0.031$ ml/min beyond which our model predicts gelation. The largest diene flow rate in our synthesis (0.02 ml/min) is about 33% lower than this critical flow rate (because of the variation of active catalyst concentration between samples, there is some uncertainty in defining the critical diene flow for the different samples).

The second and more stringent requirement on diene flow rate dictates the reproducibility in the synthesis. In figure 10(b), we consider a 5% variability in the active catalyst concentration around [Y]=10^{-6} mol/L (This is equivalent to a variation of ethylene conversion between 0.954 and 0.958). This variation in [Y] at a fixed diene feed rate changes the concentration of the different species in the reactor (and also to some extent the termination rate constant due to varying monomer concentrations) resulting in differences in the molar mass of the produced resin. At a diene flow-rate of 0.02 ml/min, the variation in M_W is about 4.5% and in M_Z is about 14%. Because of the exponential dependence of the variability of the molar mass moments at a fixed variation of [Y] as a function of the diene feed rate (figure 10b), the molar mass of the produced resin will become quite unpredictable much before the gel-point is reached.

5. Summary and discussion

In this paper, we reported the controlled terpolymerization of ethylene, α-olefin, and non-conjugated diene in a CSTR. The samples were characterized extensively and the results from the different experiments were integrated in a computer model yielding detailed branching information, and the prediction of flow-properties. The metallocene catalyst used for these

syntheses allows significant branching from macromonomer incorporation. Copolymerization with diene only marginally increases the number averaged density of branch-points as gelation is approached. Theoretically, it is predicted[12] that the number, weight, and the z-averaged molar mass remain finite at the gel-point for ethylene, diene copolymerization in CSTR. The ability to describe all the experimental results within a unified computer model demonstrates the validity of the theoretical description.

To quantitatively describe the experimental results, we needed to consider two subpopulations of ideal single-site metallocene catalysts. The minority component describes the polymerization close to the monomer inlet with higher than average monomer concentration and consequent propensity to generate short, predominantly linear chains. The primary component can incorporate macromonomers generated by either of the two subpopulations. We have used three parameters, namely the active catalyst concentration, the termination rate, and the relative concentration of the minority catalyst population as fitting parameters to describe the synthesis. For the prediction of the flow properties, the entanglement time is used as a fitting parameter. However, the linear dependence of the termination rate on the monomer concentration (Appendix B, Figure 13c) and the power-law dependence of the entanglement molar mass on the effective monomer molar mass (Figure 9) show that only the active catalyst concentration and the relative concentration of the minority catalyst population are sufficient to quantitatively describe both the polymerization process and the flow-properties of the synthesized resins.

The samples containing diene show significantly higher viscosity, stronger shear thinning and larger extension hardening compared to the sample synthesized without diene under similar conditions. The incorporation of α-olefin comonomers has been shown to be unaffected by the presence of diene. Since the concentration of diene remains extremely low, this reaction can

be used to synthesize ideal flow-modifiers that are locally indistinguishable, and hence will not phase separate from linear low-density polyethylene with arbitrary α-olefin comonomers.

We also showed that, once calibrated with the experiments, the computer model can be extended to conditions where direct experiments are difficult or unadvisable, for example to avoid reactor fouling. Using the computer models, we extend the experimental results to locate the critical diene concentration for gelation. The highest diene concentrations used in our study is about 33% lower than the critical diene concentration.

In any physical synthesis, some degree of variability in the reactor conditions is unavoidable. Using our computer model, we show that any such variability (modelled as 5% variability in the active catalyst concentration) has an exponentially large effect on the higher moments of the molar mass distribution as gelation is approached. Hence, integrated computer models incorporating variability in synthesis conditions, like the one described in this work, are invaluable for successfully avoiding reactor fouling while reaching high enough concentration of branching to significantly change the flow-properties.

Appendix

A. Limitations of ideal single-site metallocene models

The molecules generated by an ideal single site metallocene in CSTR are characterized using just two independent measures. In **figure 11**(a), we show that a choice of $M_W = 8.14 \times 10^4$ g/mol, and $\lambda = 0.22$ describes the molar mass distribution reasonably well. The model underpredicts the experimental abundance of low molar mass molecules. This can be accounted for by considering two independent components (figure 11c): the first component being an ideal single site metallocene polymer at 94 weight% characterized by $M_W = 8.35 \times 10^4$ g/mol, and $\lambda = 0.20$; and the second being a linear low density species with $M_W = 8.8 \times$

10^3 g/mol, and PDI = 2. Both of these choices give very similar radius of gyration contraction factors and rheological responses (see Figure 11b for the first choice and Figure 11d for the second choice).

However, both choices give a number of LCB/1000C which is approximately half of the value determined from NMR experiments. The NMR predicted branching can be matched by allowing the short linear molecules to be incorporated as macromonomer. The resulting coupled model produces results that also match the experimentally determined radius of gyration contraction factor (Figure 3a) and the high-frequency rheological responses (Figure 5) better.

The dashed lines in **Figure 12** shows the predictions for stress growth coefficient during uniaxial extension using the independent blend of linear and branched fractions as in Figure 11c. The predictions for non-linear extension is significantly superior when using the coupled model (solid lines) as in the main text.

B. Fitting of the rate constants

In this section, we describe an alternate fitting strategy for the syntheses that we have considered. If we assume a fixed catalyst concentration, the addition rate constants vary significantly between the different samples (**Figure 13**a). However, the computed addition rate constants for the ethylene and for the comonomer show linear correlations, suggesting the simpler alternative of fixed rate constants but varying active catalyst concentration between the samples.

Assuming fixed addition rate constants, we can calculate the ratio of active catalyst concentrations during the syntheses of the different samples from the observed conversions of

either ethylene or comonomer. In the absence of any uncertainty in the measured conversions, the catalyst concentration should be the same from computation using either of these two conversions (ethylene or comonomer). The circles in Figure 13b show that the two approaches give reasonably close results. The catalyst concentrations used in our calculations from fitting the molar mass distribution (triangles in Figure 13b) have similar scatter as the values computed from the conversions of ethylene and comonomer.

In our fitting procedure, we needed to vary the termination rates between the samples. Figure 13c shows that the termination rate constant is well-described by a linear function of the monomer concentration in the reactor. This suggests a significant contribution in the termination rates from transfer to monomer and explains the need for tuning the termination rates for each sample individually in our model that considers only unimolecular termination events.

C. Comparison of LCB prediction with NMR results

The table 4 in the main text considers only the rheologically active LCB. NMR measurements can distinguish long chain branches from incorporated hexene, but cannot separately identify pendant dienes. The LCB peak between 38.20 and 38.26 ppm encompasses the predicted shift from pendant dienes at 38.21 ppm. Similarly each of the four functional branch point in our modelling is counted as two branched carbons in NMR measurements. **Table 5** shows that accounting for these rheologically unimportant branches brings the LCB predictions from our modelling in very good agreement with the NMR results except for EDH3.

Acknowledgements: We thank Gabor Kiss, Thomas Sun and João Soares for useful discussions. The computation for this work was undertaken on ARC2, part of the high performance computing facilities at the University of Leeds, UK.

Received: Month XX, XXXX; Revised: Month XX, XXXX; Published online:

DOI: 10.1002/mren.((insert number))

Keywords: non-conjugated diene terpolymer, polymer synthesis, rheology, flow modifier, long-chain branching

[1] H. Münstedt, S. Kurzbeck, J. Stange, *Polym. Eng. Sci.* **2006**, *46*, 1190.

[2] G. J. Nam, J. H. Yoo, J. W. Lee, *J. Appl. Polym. Sci.* **2005**, *96*, 1793.

[3] D. J. Read, D. Auhl, C. Das, J. den Doelder, M. Kapnistos, I. Vittorias, T. C. B. McLeish, *Science* **2011**, *333*, 1871.

[4] H. Braunschweig, F. M. Breitling, *Coordination Chemistry Revie*ws **2006**, *250*, 2691.

[5] G. J. P. Britovsek, V. C. Gibson, D. F. Wass, *Angew. Chem. Int. Ed*. **1999**, *38*, 428.

[6] J. B. P. Soares, A. E. Hamielec, *Macromol. Theory Simul.* **1996**, *5*, 547.

[7] E. Kokko, P. Lehmus, R. Leino, H. J. G. Luttikhedde, P. Ekholm, J. H. Näsman, J. V. Seppälä*, Macromolecules* **2000***, 33,* 9200*.*

[8] C. T. Elston, US Patent 3984610, **1976**.

[9] R. P. Duttweiler, M. J. Krause, F. Y. K. Lo, S. M. C. Ong, P. P. Shirodkar, US patent 6509431, **2003**.

[10] P. J. Flory, *J. Am. Chem. Soc.* **1941**, 63, 3083.

[11] W. H. Stockmayer, *J. Chem. Phys.* **1943**, 11, 45.

[12] C. Das, D. J. Read, J. M. Soulages, P. P. Shirodkar, *Macromol. Theory Simul*. **2017**, *26*, 1700006*.*

[13] E. Kokko, P. Pietikäinen, J. Koivunen, J. V. Seppälä, *J. Poly. Sc. Poly. Chem.* **2001**, *39*, 3805.

[14] N. Naga, Y. Imanishi, *Macromol. Chem. Phys*. **2002**, *203*, 2155.

[15] M. de Fátima V. Marques, D. Ramos, J. D. Rego, *Euro. Poly. J*. **2004**, *40*, 2583.

[16] J. D. Guzmán, D. J. Arriola, T. Karjala, J. Gaubert, B. W. S. Kolthammer, *AIChE J*. **2010**, *56*, 1325.

[17] Z. Ye, F. AlObaidi, S. Zhu, *Ind. Eng. Chem. Res*. **2004**, *43*, 2860.

[18] R. Li, A. B. Corripio, K. M. Dooley, M. A. Henson, M. J. Kurtz, *Chem. Eng. Sci*. **2004**, *59*, 2297.

[19] R. C. S. Dias, M. R. P. F. N. Costa, *Macromol. React. Eng*. **2007**, *1*, 440.

[20] M. Nele, J. B. P. Soares, J. C. Pinto, *Macromol. Theory Simul.* **2003**, *12*, 582.

[21] G. ver Strate, C. Cozewith, W. W. Graessley, *J. Appl. Polymer Sc*. **1980**, *25*, 59.

[22] T. Sun, P. Brant, R. R. Chance, W. W. Graessley, *Macromolecules* **2001**, *34*, 6812.

[23] T. Sun, R. R. Chance, W. W. Graessley, D. J. Lohse, *Macromolecules* **2004**, *37*, 4304.

[24] B. Monrabal, J. Sancho-Tello, N. Mayo, L. Romero, *Macromol. Symp*. **2007**, *257*, 71.

[25] J. C. Randall, J. Macromol. Sci., Part C, *Polymer Reviews* **2006**, *29*, 2006.

[26] W. Liu, D. G. Ray, P. L. Rinaldi, *Macromolecules* **1999**, *32*, 3817.

[27] K. Klimke, *PhD Thesis*, Universität Mainz **2006**. http://publications.ub.uni-mainz.de/theses/volltexte/2006/1077/pdf/1077.pdf

[28] K. Klimke, M. Parkinson, C. Piel, W. Kaminsky, H. W. Spiess, M. Wilhelm, *Macromol. Chem. Phys*. **2006**, 207, 382.

[29] A. Schöbel, E. Herdtweck, M. Parkinson, B. Rieger, *Chem. Eur. J*. **2012**, 18, 4174.

[30] C. Das, D. J. Read, J. M. Soulages, P. P. Shirodkar, *Macromolecules* **2014**, *47*, 5860.

[31] H. Tobita, A. E. Hamielec, *Polymer* **1991**, *32*, 2641.

[32] D. J. Read, T. C. B. McLeish, *Macromolecules* **2001**, *34*, 1928.

[33] C. Das, N. J. Inkson, D. J. Read, M. A. Kelmanson, T. C. B. McLeish, *J. Rheol*. **2006**, *50*, 207.

[34] C. Das, D. J. Read, D. Auhl, M. Kapnistos, J. den Doelder, I. Vittorias, T. C. B. McLeish, *J. Rheol*. **2014**, *58*, 737.

[35] bob2.5. http://sourceforge.net/projects/bob-rheology, **2012**, accessed October, 2018.

[36] M. Doi, S. F. Edwards, *The theory of polymer dynamics*, Clarendon Press, Oxford, **1986**.

[37] P. G. de Gennes, *J. Chem. Phys*. **1971**, *55*, 572.

[38] T. C. B. McLeish, *Europhys. Lett*. **1988**, *6*, 511.

[39] G. Marrucci, *J. Polym. Sci. Polym. Phys. Ed*. **1985**, *23*, 159.

[40] R. G. Larson, *Macromolecules* **2001**, *34*, 4556.

[41] E. van Ruymbeke, C. Bailly, R. Keunings, D. Vlassopoulos, *Macromolecules* **2006**, *39*, 6248.

[42] T. C. B. McLeish, R. G. Larson, *J. Rheol*. **1998**, *42*, 81.

[43] L. J. Fetters, D. J. Lohse, C. A. García-Franco, P. Brant, D. Richter, *Macromolecules* **2002**, *35*, 10096.

[44] X. Chen, F. J. Stadler, H. Münstedt, R. G. Larson, *J. Rheol*. **2010**, *54*, 393.

[45] R. G. Almo, L. Mandelkern, *Thermochimica Acta* **1994**, *238*, 155.

[46] M. Nele, J. B. P. Soares, *Macromol. Theory and Sim*. **2002**, *11*, 939.

[47] N. J. Inkson, C. Das, D. J. Read, *Macromolecules* **2006**, 39, 4920.

[48] F. J. Stadler, H. Münstedt, *J. Rheol*. *2008*, **52**, 697.

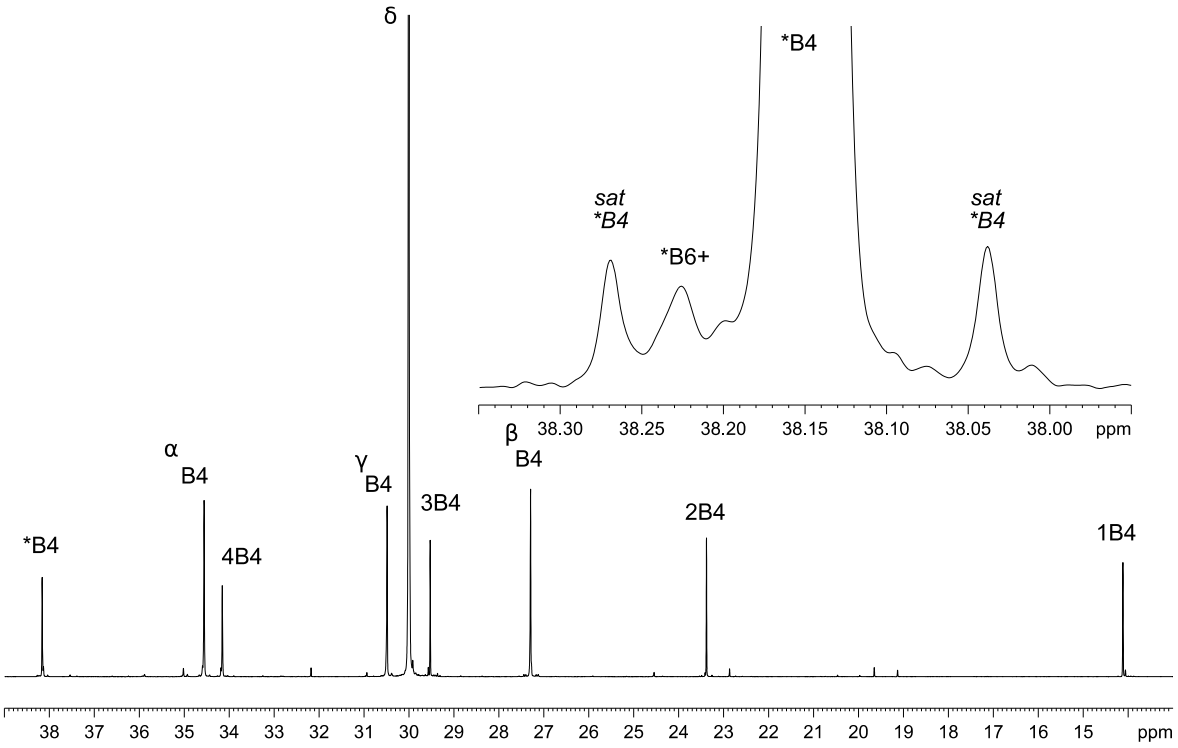

Figure 1. ^{13}C NMR spectrum for EDH1. A Magnified plot of the region around the peak assigned to long chain branches is shown in the inset.

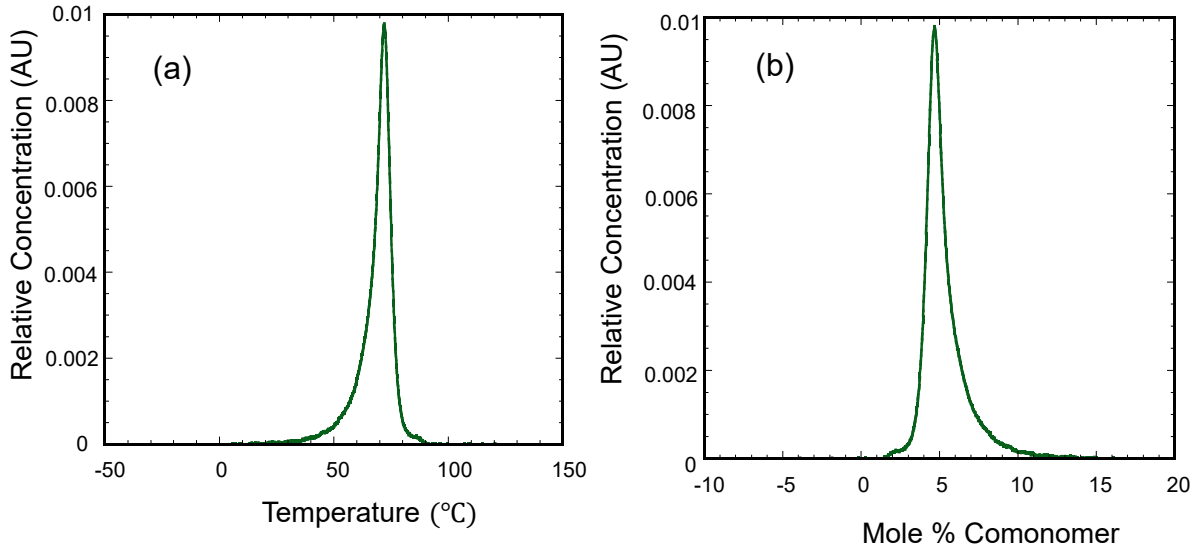

Figure 2. (a) Crystallizable fraction as a function of temperature, and (b) relative concentration of molecules as a function of the mole fraction of hexene.

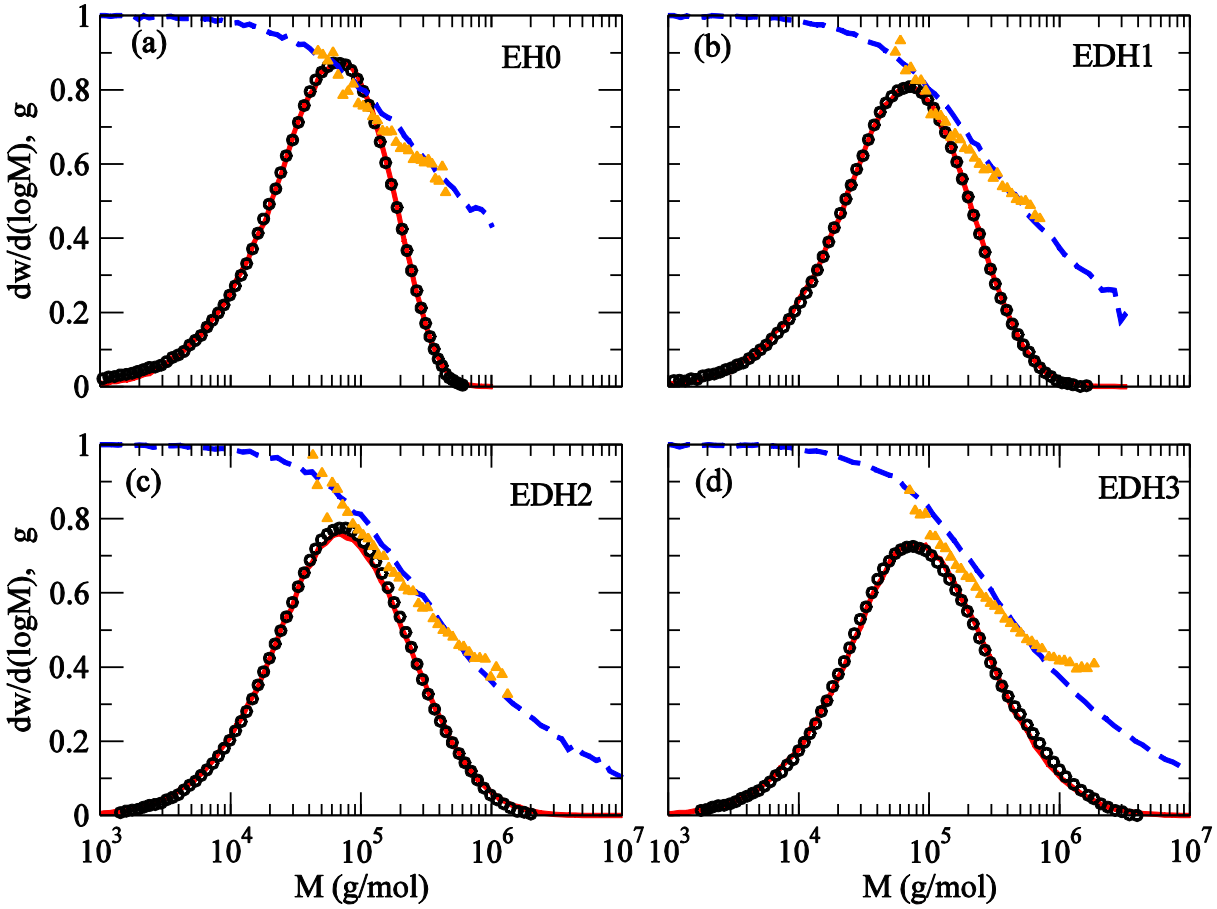

Figure 3. Experimental (lines) and model (symbols) cumulative molar mass distributions and radius of gyration contraction factors for the ethylene-hexene polymers.

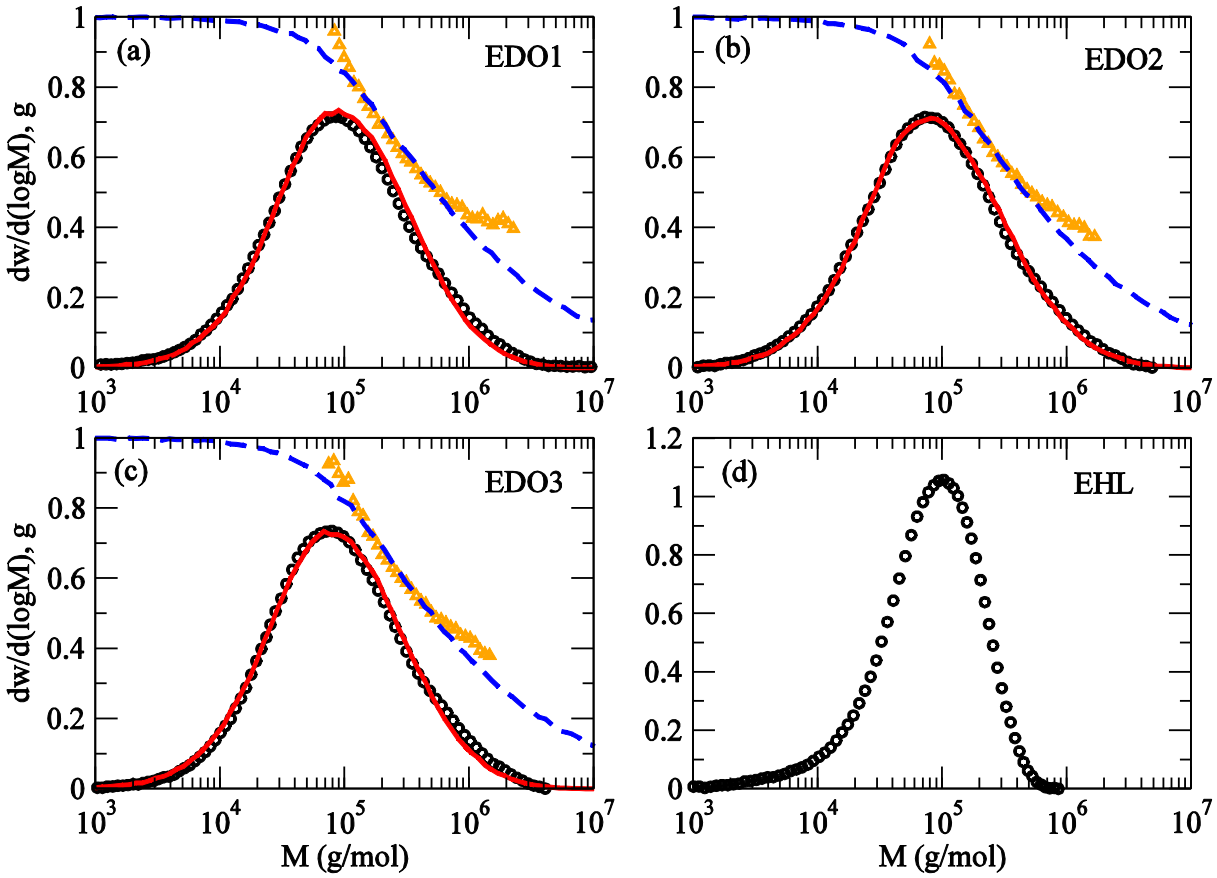

Figure 4. Experimental (symbols) and model (lines) molar mass distributions and radius of gyration contraction factors for the ethylene-diene-octene copolymers and the linear polymer EHL. The experimental molar mass distribution for EHL was discretized to directly generate the numerical ensemble for rheology prediction.

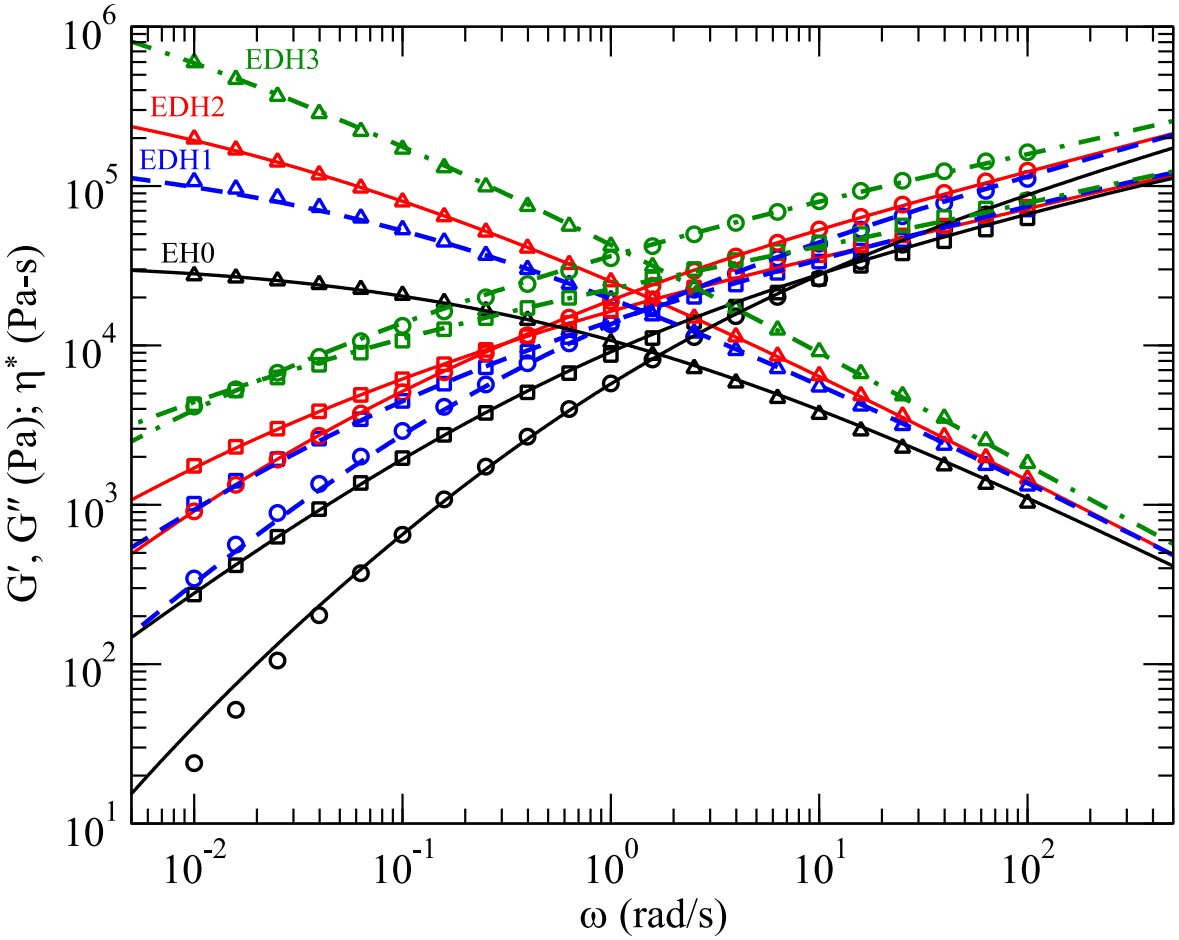

Figure 5. Small amplitude oscillatory shear response of the ethylene-hexene resins: the symbols are from experiments at 190°C and the lines are the model predictions.

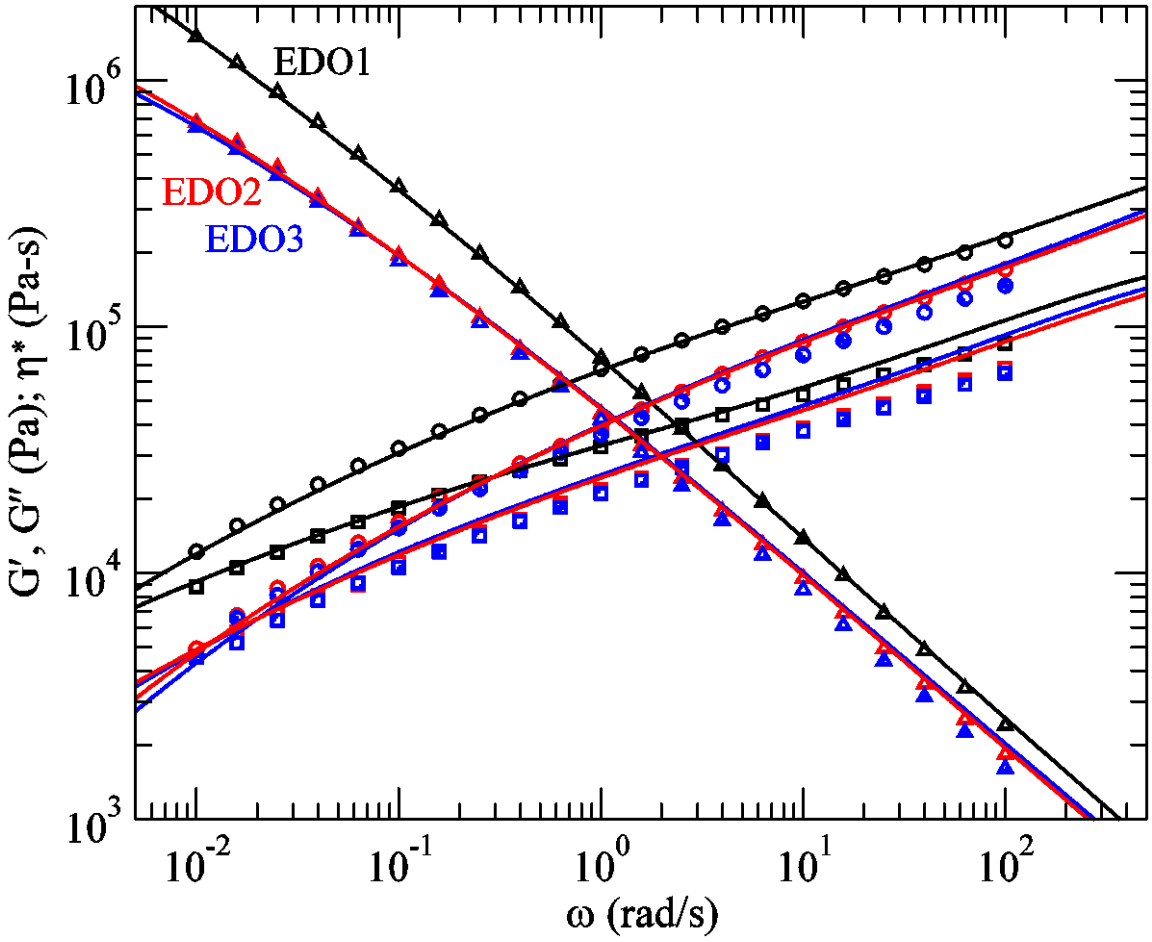

Figure 6. Small amplitude oscillatory shear response of the ethylene-octene resins: the symbols are from experiments at 190°C and the lines are the model predictions.

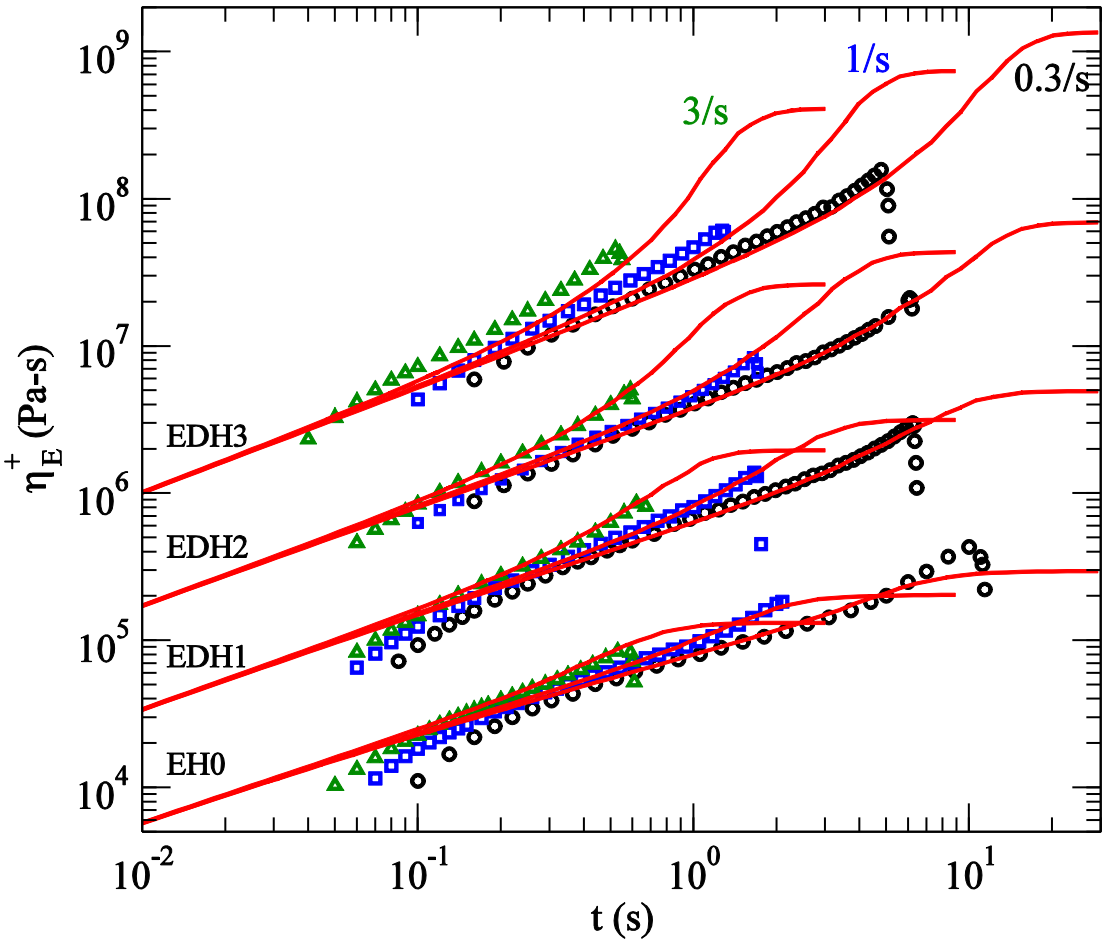

Figure 7. Experimental data (symbols) and model predictions (lines) for the start-up stress growth coefficients (transient viscosities) in uniaxial extensional flow for the ethylene-hexene resins. For clarity, the data for EDH1, EDH2, and EDH3 have been shifted vertically by a factor of 5, 25 and 125, respectively.

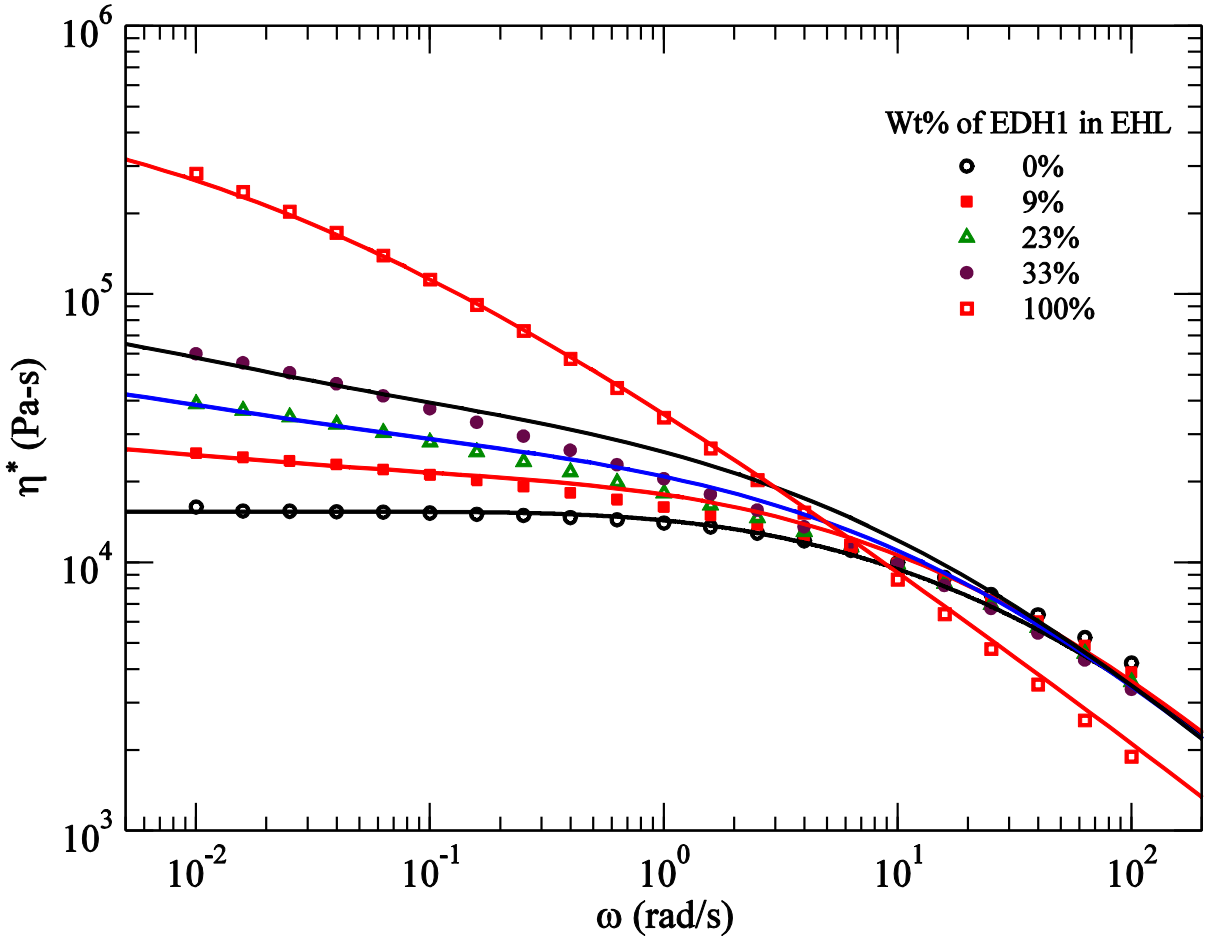

Figure 8. Dynamic viscosity obtained from small amplitude oscillatory shear experiments for the blends of EDH1 in EHL at the shown weight fractions: the symbols are from experiments at 150℃ and the lines are the model predictions.

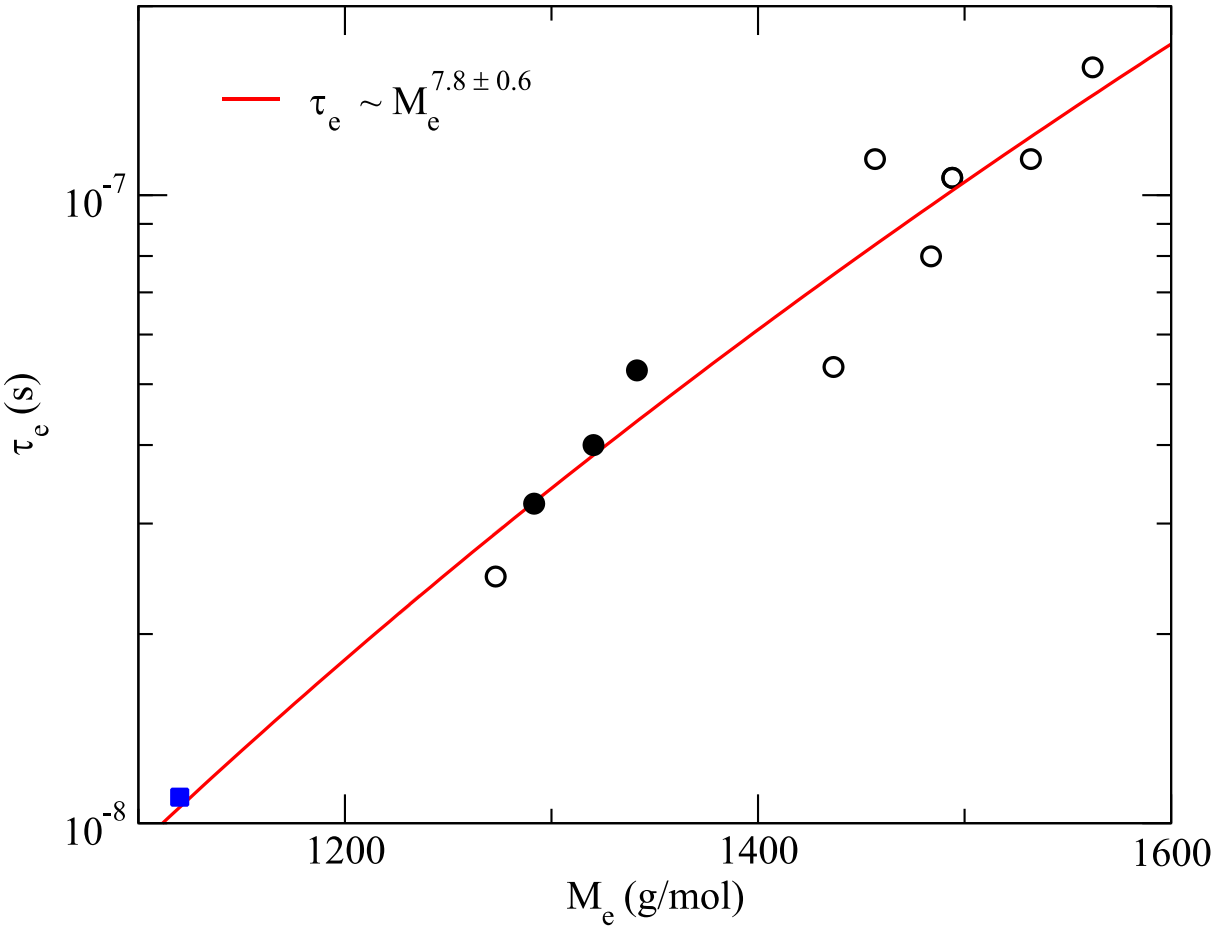

Figure 9. Choice of τ_e and M_e to fit the rheology data at 150°C. The fit is a power-law with exponent 7.8 ± 0.6. The filled square is literature data for comonomer-free metallocene polyethylene at 150°C [33]. The open and filled circles respectively are for the as synthesized polymers and for the blends.

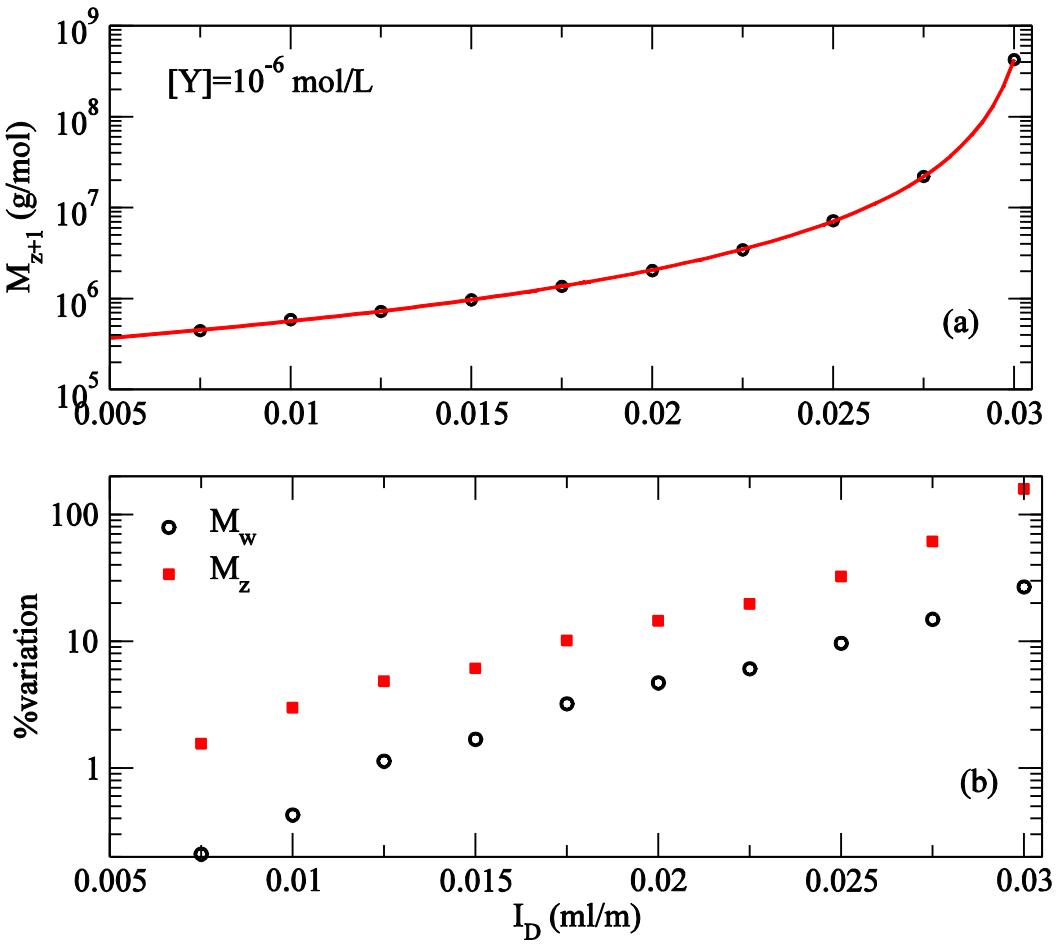

Figure 10. (a) Scaling of Z+1 moment of the molar mass with increasing diene feed concentration. The fit (solid line) gives a critical diene feed concentration of 0.031 ml/min for the onset of gelation. (b) Typical expected variation in M_W and M_Z between batches with ±5% variation in the active catalyst concentration.

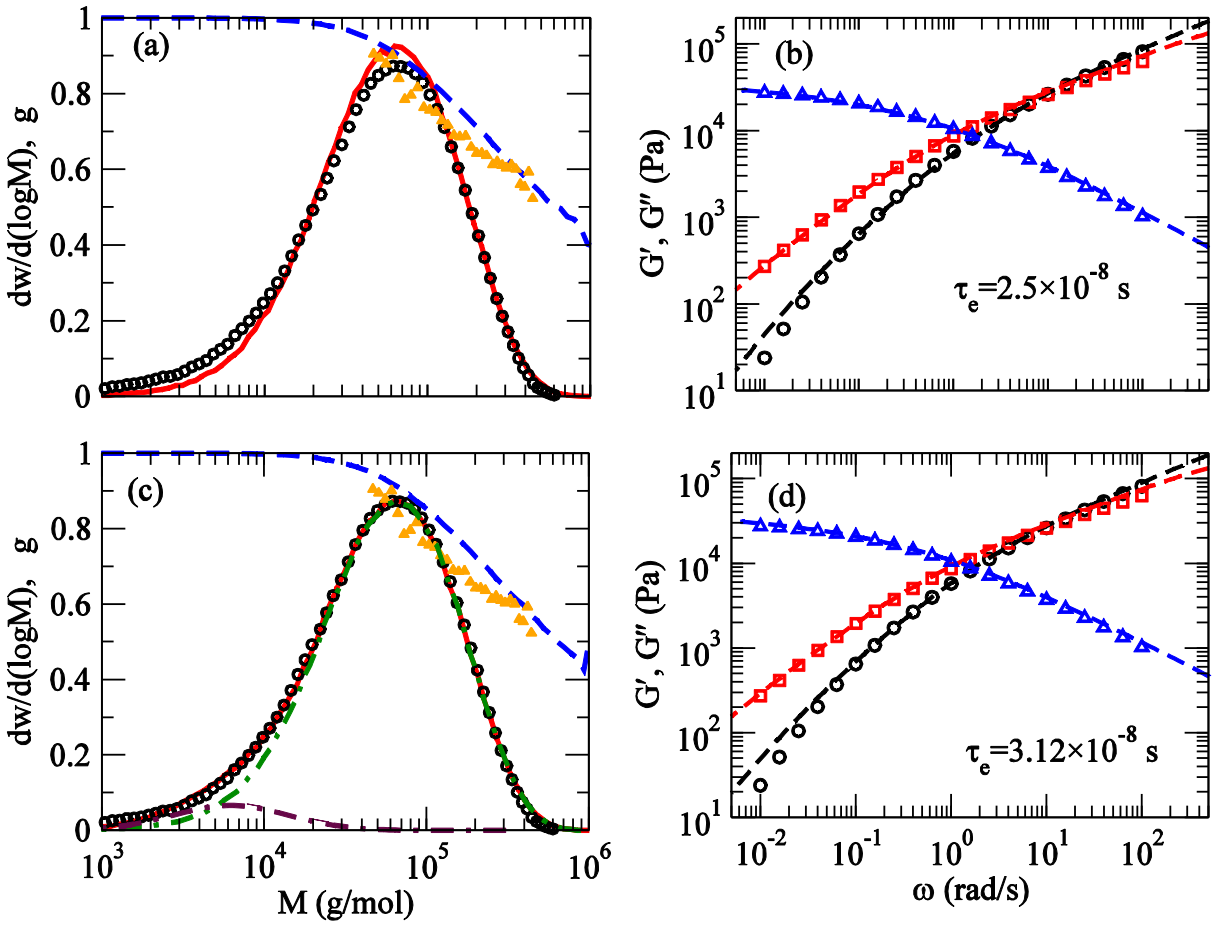

Figure 11. (a) Predicted molar mass distribution and (b) frequency response for an ideal single site metallocene in CSTR. (c) Molar mass distribution and (d) frequency response from a blend of ideal single site metallocene polymers and a small fraction of short linear polymers. The contributions from the individual components are shown as dot-dashed lines in (c). In all cases, the lines are the model predictions and the symbols represent the experimental data.

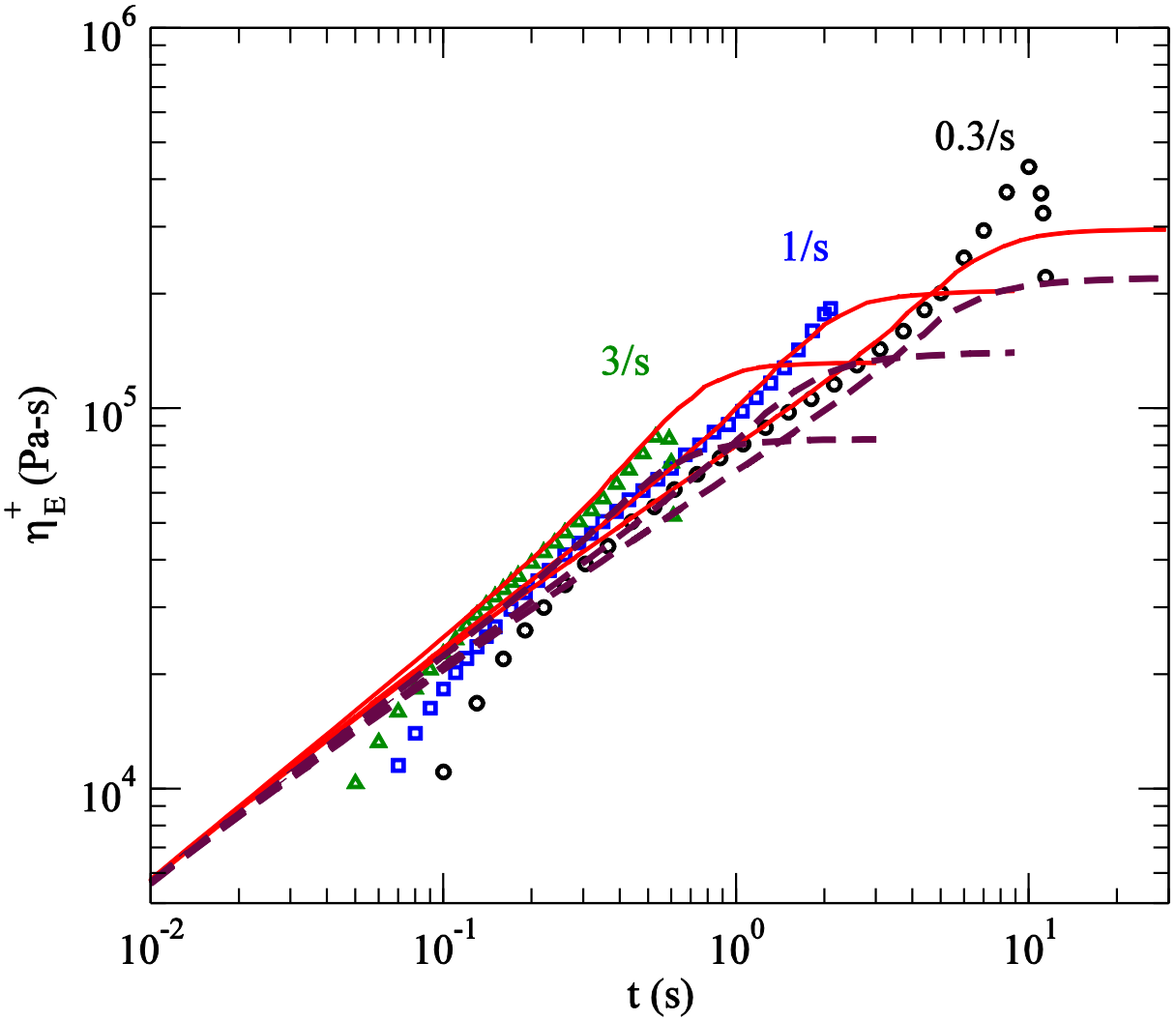

Figure 12. Transient response in uniaxial extension for EH0 at the shown rates. The symbols are the experimental data, the solid lines are predictions assuming coupled catalysts as in the main text and the dashed lines are predictions from blends of independent branched single site metallocene and linear species as in figure 11c.

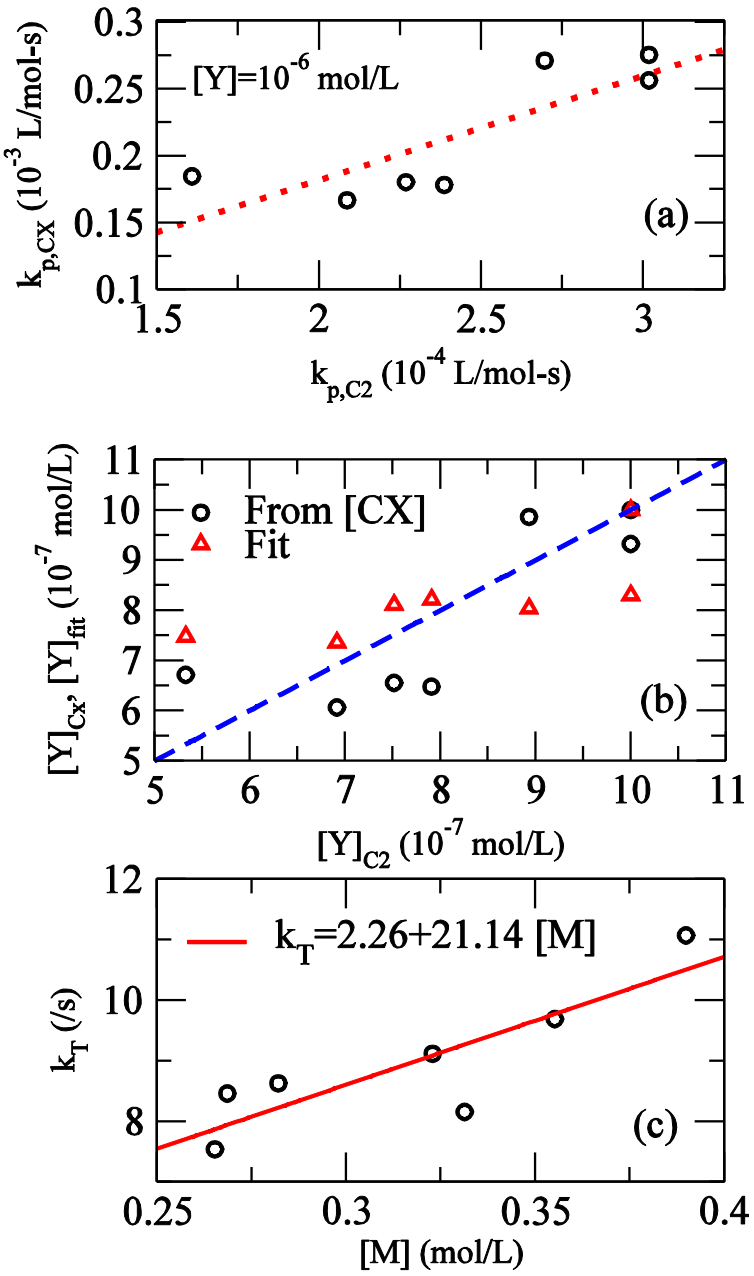

Figure 13. (a) Monomer and comonomer propagation rate constants for the different samples calculated by assuming a fixed catalyst concentration [Y]=10^{-6} mol/L. The dotted line is a guide to the eye. (b) Circles: Assuming constant rate constants and [Y]=10^{-6} mol/L for EH0, the catalyst concentration calculated from the conversion of ethylene vs. catalyst concentration calculated from conversion of comonomer. Triangles: catalyst concentrations from our fitting procedure. (c) The fitted values for the (total) termination rate constant shows a linear trend on the concentration in the reactor.

Table 1. Comonomer and diene feed rates and conversion of ethylene and comonomer.

Resin	Comonomer type	Comonomer rate (g/min)	Diene rate (g/min)	Ethylene conversion (%)	Comonomer conversion (%)
EH0	hexene	1.8	0	95.6	66.5
EDH1	hexene	1.8	0.01	95.1	66.1
EDH2	hexene	1.8	0.015	95.6	64.9
EDH3	hexene	1.8	0.02	94.5	56.2
EDO1	octene	1.6	0.02	92.1	57.1
EDO2	octene	2.0	0.02	94.2	56.5
EDO3	octene	2.2	0.02	93.8	54.6

Table 2. Molar mass moments from SEC-MALLS, viscosity contraction factors (g′), crystallization and melting temperatures, and enthalpy of melting from DSC.

Resin	M_N (kg/mol)	M_W (kg/mol)	M_Z (kg/mol)	g′ (vis-av.)	T_c (C)	T_m (C)	ΔH (J/g)
EH0	23.4	82.3	162.4	0.80	85.91	104.31	107.1
EDH1	25.1	104.8	255.7	0.75	85.41	104.40	105.1
EDH2	32.2	126.2	356.4	0.73	85.96	104.97	105
EDH3	35.2	172.0	619.4	0.68	89.97	108.18	110.9
EDO1	30.5	226.5	2040.8	0.67	95.30	114.65	112.5
EDO2	37.2	201.1	946.6	0.67	91.42	110.65	118.9
EDO3	34.1	204.1	1068.3	0.66	90.87	109.44	117.6

Table 3: Number of double bonds and long chain branches per 1000 carbons from ^{1}H and ^{13}C NMR.

	^{1}H NMR				^{13}C NMR	
	-CH=CH2	-CH=CH-	-CH=C<	>C=CH2	-CH=CH2	LCB
EH0	0.14	0.21	0.29	0.07	0.11	0.39
EDH1	0.15	0.14	0.21	0.07	0.12	0.40
EDH2	0.18	0.20	0.28	0.05	0.13	0.42
EDH3	0.17	0.08	0.07	0.04	0.18	0.51

Table 4. Molar concentrations of ethylene and comonomer in the reactor, fitted values of the mole fraction of the 2nd catalyst φ_{Y2}, total termination rate constant for the primary catalyst $k_T \equiv k^{=} + k_s$, the catalyst concentration [Y], and the number of LCB/1000C (λ), number of LCB per molecule (b_m), number of terminal double bonds ($n^{=}$), and the effective monomer molar mass (M_0).

Resin	**[C2] (mol/L)**	**[Cx] (mol/L)**	$\boldsymbol{\varphi_{Y2}}$	$\boldsymbol{k_T}$ **(/s)**	**[Y] /10^{-6} (mol/L)**	**λ**	$\boldsymbol{b_m}$	$\boldsymbol{n^{=}}$	**M0 (g/mol)**
EH0	0.175	0.086	0.16	8.46	1	0.39	0.63	0.13	30.41
EDH1	0.195	0.087	0.14	8.63	0.804	0.35	0.66	0.16	30.41
EDH2	0.175	0.090	0.13	7.54	0.830	0.35	0.72	0.18	30.35
EDH3	0.219	0.113	0.13	8.16	0.822	0.31	0.74	0.17	30.07
EDO1	0.316	0.073	0.05	11.07	0.748	0.27	0.81	0.12	30.15
EDO2	0.230	0.093	0.06	9.12	0.811	0.31	0.84	0.14	30.63
EDO3	0.248	0.107	0.07	9.69	0.736	0.30	0.78	0.09	30.80

Table 5. Comparison of branching contents from modelling and from NMR. NMR measurements count each four functional branch points (H-branches) as two separate branched carbons. Similarly pendant dienes (C10) are counted as long chain branches.

	EH0	**EDH1**	**EDH2**	**EDH3**
T-branch	0.385	0.336	0.328	0.286
H-branch	-	0.012	0.021	0.023
Pendant C10	-	0.039	0.064	0.069
T + 2*H + C10	0.39	0.40	0.43	0.40
NMR	0.39	0.40	0.43	0.51

Table of content entry

Integrated computer modelling of synthesis and characterization reveals the detailed branching structures in a set of ethylene-diene copolymers. Controlled synthesis is achieved for different concentrations of diene and another comonomer. Combining multiple experiments and modelling enhances the understanding about the synthesis and allows to theoretically determine the appropriate reactor conditions for polymers with given desired flow properties.

Chinmay Das*, Muhiddin Elguweri, Peijun Jiang, Shuhui Kang, Mauritz Kelchtermans, Tom C. B. McLeish, Matthew Parkinson, Daniel J. Read*, Michael P. Redlich, Pradeep P. Shirodkar, Johannes M. Soulages

Controlled synthesis, characterization, and flow-properties of ethylene-diene copolymers